

Article

Creep Characteristics of Reconstituted Silty Clay under Different Pre-Loading Path Histories

Bin Xiao ^{1,2,*} , Peijiao Zhou ^{2,3} and Shuchong Wu ²

¹ Department of Art and Design, Zhejiang Tongji Vocational College of Science and Technology, Hangzhou 311231, China

² Department of Civil Engineering, Zhejiang University of Technology, Hangzhou 310014, China; pjzhouzjut@163.com (P.Z.); wullish@126.com (S.W.)

³ Department of Engineering Cost, Zhejiang College of Construction, Hangzhou 311231, China

* Correspondence: 2111406048@zjut.edu.cn

Abstract: Due to the long-term deformation settlement of foundations, issues such as damage and functional failure of buildings and structures have long been a concern in the engineering field. The creep of soil is one of the primary causes leading to long-term deformation of foundations. In this paper, the consolidation deformation, creep characteristics, and creep model of reconstituted saturated silty clay were studied using the isotropic consolidation creep test and triaxial compression creep test. The results show that for the isotropic consolidation creep test, although the applied load adopted different stages of loading, as long as the final applied confining pressure was the same, the number of stages applied by the confining pressure had little effect on the final isotropic consolidation deformation of the sample and the triaxial undrained shear strength after creep. However, for the triaxial shear creep test, it was found that under the same final deviatoric stress, the final deviatoric strain of the sample was closely related to the number of loading stages of deviatoric stress. The test showed that the more loading stages with the same deviatoric stress, the smaller the final deviatoric strain, and the triaxial undrained shear strength of the sample after creep increased. In addition, it was reasonable to set the pore pressure dissipation of the sample at 95% ($(u_0 - u)/u_0 = 95\%$) as the time (t_{100}) at which the primary consolidation of the soil sample was completed. The isotropic consolidation creep curves and the triaxial compression creep curves showed certain non-linearity. Then, the logarithmic model and the hyperbolic model were used to fit the creep curves of the samples. It was found that the hyperbolic model had a better fitting effect than the logarithmic model, but for the triaxial compression creep test, the creep parameters of the sample changed greatly. Therefore, studying the creep characteristics of soil under different pre-loading steps is of significant engineering importance for evaluating the long-term deformation of underground structures.

Keywords: reconstituted silty clay; isotropic consolidation; triaxial compression; loading steps; creep model



Citation: Xiao, B.; Zhou, P.; Wu, S. Creep Characteristics of Reconstituted Silty Clay under Different Pre-Loading Path Histories. *Buildings* **2024**, *14*, 1445. <https://doi.org/10.3390/buildings14051445>

Academic Editors: Mingming He and Yonggang Zhang

Received: 8 April 2024

Revised: 6 May 2024

Accepted: 13 May 2024

Published: 16 May 2024



Copyright: © 2024 by the authors. Licensee MDPI, Basel, Switzerland. This article is an open access article distributed under the terms and conditions of the Creative Commons Attribution (CC BY) license (<https://creativecommons.org/licenses/by/4.0/>).

1. Introduction

The mechanical behavior of clay is highly time-dependent. The time-dependence of clay results in long-term ground settlement/deformation, which threatens the safety and serviceability of the buildings/structures built in/on it, especially when the foundation is predominantly cohesive soils.

In previous studies [1–20], undisturbed and reconstituted soil samples were tested to investigate their creep behaviors under different loading paths, stress levels, etc. Also, influential factors, such as temperature and strain rate, were identified [21–24]. Augustesen et al. [1] and Zhu et al. [2] elucidated that clay under constant effective stress manifests significant secondary consolidation, with the axial strain or void ratio linearly correlating with the logarithm of time. The secondary consolidation coefficient (C_α), integral to

this characterization, is associated with the compression index (C_c). Furthermore, the creep coefficient (C_α) was found to decrease with a diminishing void ratio, with its value being substantially influenced by the integrity of interparticle bonds. Bishop et al. [3] performed drained creep tests on undisturbed overconsolidated London clay and normally consolidated Pancone clay, noting unstable creep rate fluctuations potentially linked to structural changes. They observed creep deformation across all stress levels without a definable threshold. Fodil et al. [4], through triaxial creep testing, explored the secondary consolidation and creep behavior of soft clay, finding that these rates are closely tied to the loading rate, with consistent viscoelastic responses irrespective of the stress levels or paths. Xiao [5] and Hu et al. [6,7] conducted drained triaxial creep tests on both normally and overconsolidated clayey soils, identifying hyperbolic time-deformation curves under constant deviatoric stress for both soil types. Leroueil et al. [8] and Jostad et al. [9] provided insights into the non-linear creep behavior of soft clay, revealing that the creep rate is tied to the stress magnitude and path. The correlation between secondary consolidation pressure and strain rate under varied stress levels is unique to each specimen and is normalizable for consistent representation. Vyalov et al. [10], through triaxial compression testing on stiff clay, identified distinct creep behaviors in the pre- and post-critical states. They formulated equations to characterize both fading and non-fading creep, incorporating the effects of expansiveness on the soil's volumetric strain. Maria et al. [21], Miao et al. [22], Mesri [23], and Newland et al. [24] identified strain rate as a key determinant of clayey soil creep behavior. Collectively, their research showed that soil remolding attenuates creep rates, with visco-plastic models adeptly characterizing viscosity during primary consolidation and the elastoplastic strain's influence on yield. Furthermore, temperature is recognized for its significant impact on compression rates, which is more pronounced than its effect on the creep coefficient itself. Wang et al. [11], Zeng et al. [12], and Wu et al. [13] executed one-dimensional consolidation compression tests on various reconstituted soil types, revealing that secondary consolidation deformation is influenced by stress levels, soil sample void ratios, and void ratios at liquid limits. Luo et al. [14], in their investigation of soft soil deformation progression over time under diverse stress paths, drainage conditions, and stress levels, conducted one-dimensional and triaxial compression creep tests. Subsequently, they developed a Merchant model enhanced with fractional derivatives to encapsulate the observed behavior. Chen [15] investigated the influence of consolidation on the mechanical properties of marine-terrestrial interlayered soft soil. The study revealed that pre-consolidation pressure diminishes the influence of soil structure on shear strength. Moreover, the consolidation state is a significant determinant of creep failure characteristics and strain rate behavior. Zhou [16] performed triaxial shear creep tests on undisturbed and reconstituted saturated clays from Hangzhou, revealing that undisturbed samples experienced greater creep and longer development times under the same deviatoric stresses. These observations underscore the influence of structure on clay's creep behavior. Various empirical creep models were proposed to describe the rheological behaviors of cohesive soils [17–19,25–31]. For example, Yin [29] proposed a widely employed logarithmic empirical model based on laboratory one-dimensional compression triaxial tests, and Singh et al. [30] proposed a power function model. Mesri et al. [31] proposed a modified Singh–Mitchell model. Xiao et al. [17] proposed an empirical hyperbolic creep model based on the triaxial shear creep test of saturated clay in Hangzhou City, with a clear physical meaning for parameters and a good fitting effect. Long et al. [18], utilizing consolidation creep tests, examined the creep characteristics of Changsha red clay and formulated an empirical model that accurately forecasts creep behavior under loads of up to 500 kPa. Concurrently, Niu et al. [19], through triaxial testing, explored the dynamic creep properties of frozen silty clay and developed a non-constant fractional dynamic creep model grounded in fractional calculus. This model adeptly simulates the rheological response of frozen soil during accelerated creep phases. These studies demonstrate that laboratory tests are effective in studying the creep behaviors of soil, and they are of great

value in establishing creep models through creep tests under deviatoric stress conditions to guide the project construction.

The above studies show that although there have been many relevant results on the creep properties of cohesive soil, the influence of loading steps under some specific loading paths that may be related to the construction schedule and management is rarely investigated. Some of these relevant research results were reported in the Proceedings of China-Europe Conference on Geotechnical Engineering [20]. The study of Teresa M. Bodas Freitas et al. [32] pointed out that a pre-loading on a foundation or embankment may cause an increase in the undrained strength of the soil, but its influence on soil displacement was not clarified. Therefore, the time-dependent deformation characteristics of soil under different loading paths need to be further studied. The study of the time-dependent deformation characteristics of soil under different loading paths is also the basis for investigating a soil creep model and its application. In this paper, isotropic consolidation creep tests and triaxial compression creep tests under different pre-loading steps were performed on the silty clay in the Taizhou area. The time-dependent deformation characteristics of the silty clay under different loading paths and the influence of grading loading were studied. The empirical model suitable for describing the creep behaviors of silty clay is discussed, and the distribution law and value suggestion of model parameters were further analyzed, which provides a basis for the deformation calculation of silty clay foundations.

2. Soil Characteristics and Specimen Preparation

The soil samples were taken from an excavation site in Taizhou located in Hangzhou Bay area of China, at depths between 20.0 m and 25.0 m. According to ISO 14688-2:2017 [33] and the Chinese National Standard GB 50007 [34], the physical and mechanical properties of the soil sample were characterized and are detailed in Table 1. The liquid limit (w_L) of the soil sample was measured at 37.9%, and the plasticity index (I_P) at 15.32%. The soil fraction with a particle size greater than 0.075 mm constituted 0.47% of the sample, the fraction between 0.005 mm and 0.075 mm made up 33.23% of the sample, and the fraction less than 0.005 mm accounted for 66.30%. The particle size distribution curve of the soil sample is illustrated in Figure 1a. Concurrently, the plasticity chart of the sample, based on the liquid limit (w_L) and plasticity index (I_P), is presented in Figure 1b. It can be observed from the plasticity chart that the data points for the soil sample lie just beneath the reference A-line and are very close to it. Based on the soil classification standards (ISO 14688-2:2017), soils above the A-line are categorized as clays, while those below are considered silts. Soil samples that fall on or very near A-line are designated as silty clays. The liquid limit range is indicative of a medium liquidity index. Consequently, the soil sample can be classified as silty clay based on this classification. Furthermore, in accordance with the Chinese National Standard GB 50007, the plasticity index (I_P) of the soil sample fell within the range of $10 < I_P = 15.32 < 17$, which also supports the classification of the soil as silty clay. The undisturbed soil samples were in a plastic state, and the specimens were reconstituted for tests in this study.

Table 1. The properties of soil specimens.

Depth/m	G_s	Water Content/%	Void Ratio	w_L /%	w_P /%	I_P	The Content of Grain/%			Soil Type
							>0.075 mm	0.005–0.075 mm	<0.005 mm	
20–25	2.72	24.45	0.668	37.90	22.58	15.32	0.47	33.23	66.30	Silty clay

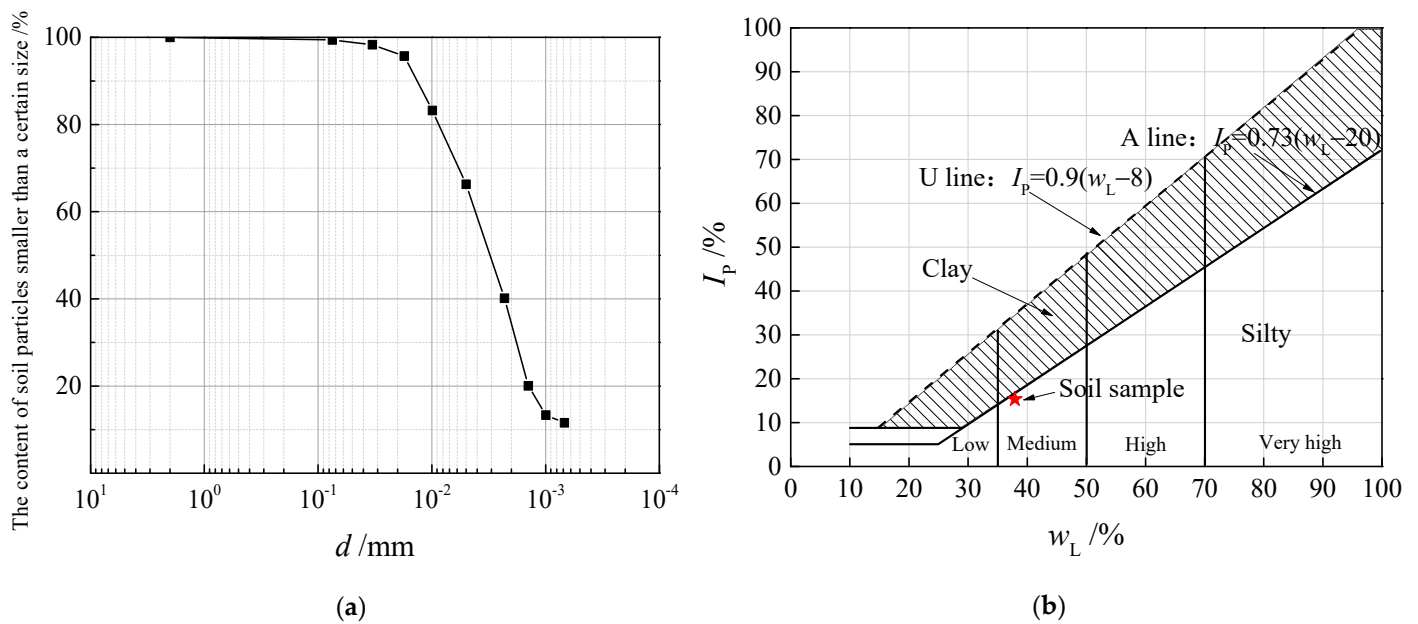


Figure 1. Particle size distribution curve and plasticity chart of the soil sample. (a) Particle size distribution curve. (b) Plasticity chart.

The tests were performed on cylindrical specimens with a diameter of 38 mm and a height of 78 mm, which were dynamically compacted into nine layers on the base of the triaxial cell. The specimens were prepared by the moist tamping method (dynamic compaction) [5] to achieve better uniformity. The reconstituted soil preparation apparatus and the prepared silty clay samples are shown in Figure 2. The apparatus included a saturator and a compaction device. The internal diameter of the saturator was 38 mm, with a height of 76 mm. The compaction device was equipped with a heavy hammer weighing approximately 295 g and a diameter of 38 mm. The drop height of the hammer, determined through extensive trials, was set at 15 cm. It was necessary to scrape the surface of each layer to ensure the uniformity of the entire sample.



Figure 2. Triaxial reconstituted soil specimen preparation apparatus and soil sample [5].

Before testing, the specimens were pre-saturated by the vacuum saturation method. The degree of saturation of the soil sample, after undergoing vacuum saturation, reached approximately 70% to 80%, which does not meet the standard recommendation that soil sample saturation should exceed 95%. Consequently, it was necessary to subject the samples

to back pressure saturation, with a back pressure of $BP = 250$ kPa; saturation control was achieved through the Skempton parameter $B = \Delta u / \Delta \sigma_3$. If the value of $B > 0.95$, the sample is considered to have satisfied the saturation requirement.

3. Test Program and Procedure

The primary objective of this study was to investigate the influence of pre-loading steps on the time-dependent deformation behavior of silty clay through a defined testing program. The reconstituted soil samples were tested under two loading paths (isotropic consolidation and triaxial shear creep tests), with all tests being conducted under drained conditions.

For the isotropic consolidation creep tests, the saturated specimens were consolidated at a constant main stress rate of $\Delta p = 10$ kPa/min to a hydraulic pressure of $p = 800$ kPa. The stresses were applied in three different steps: $\Delta p = 0 \rightarrow 800$ kPa, $\Delta p = 0 \rightarrow 400 \rightarrow 800$ kPa, and $\Delta p = 0 \rightarrow 200 \rightarrow 400 \rightarrow 600 \rightarrow 800$ kPa. For each test, the hydraulic pressure was kept constant at $p = 800$ kPa for 96 h. The loading plan of the isotropic consolidation creep tests is shown in Figure 3a. At the end of the above processes, the specimens were all sheared to failure at a constant pressure rate of $\Delta q = 4.5$ kPa/min under undrained conditions.

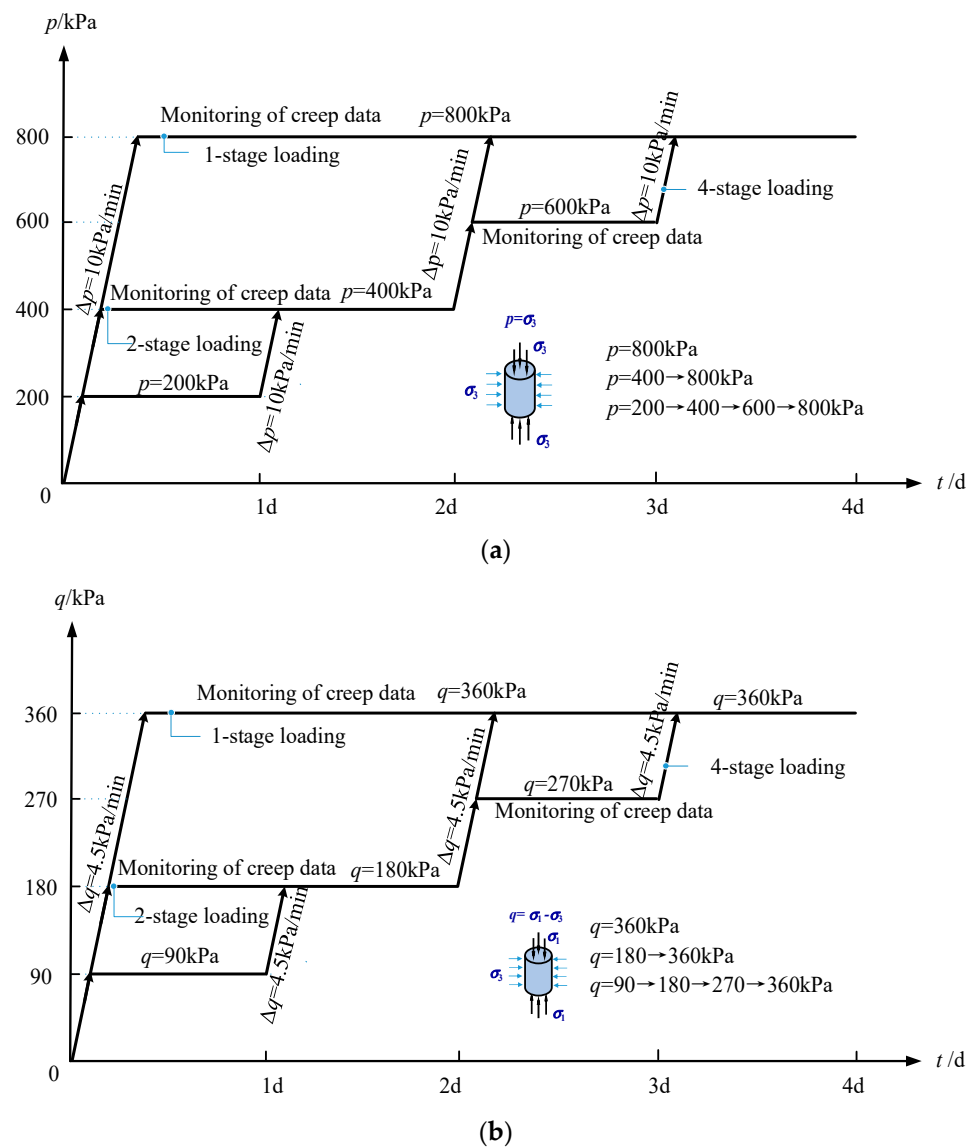


Figure 3. Load plan of the tests. (a) Isotropic consolidation. (b) Triaxial compression.

For the triaxial compression creep tests, the saturated specimens were first consolidated under an all-around pressure of $p = 800$ kPa. Then, after the excess pore water pressure dissipated, they were vertically compressed at a constant pressure rate of $\Delta q = 4.5$ kPa/min to $q = \sigma_1 - \sigma_3 = 360$ kPa. The deviatoric stresses were applied in three different steps: $\Delta q = \Delta\sigma_1 - \Delta\sigma_3 = 0 \rightarrow 360$ kPa (96 h), $\Delta q = 0 \rightarrow 180$ (48 h) $\rightarrow 360$ kPa (48 h), and $\Delta q = 0 \rightarrow 90$ (24 h) $\rightarrow 180$ (24 h) $\rightarrow 270$ (24 h) $\rightarrow 360$ kPa (24 h). The loading plan of the triaxial compression tests is displayed in Figure 3b. At the end of the above processes, the specimens were also sheared to failure at a constant pressure rate of $\Delta q = 4.5$ kPa/min under undrained triaxial conditions.

All tests were performed in a GDS servo-controlled triaxial testing system. The laboratory temperature was controlled at 23 ± 1 °C throughout the testing to eliminate the influence of temperature on the test results.

4. Creep under Total Stresses

4.1. Effect of Pre-Loading Steps on Silty Clay under Isotropic Consolidation

Figure 4 shows the development of volumetric strain (ε_v) and the variation in pore water pressure (u) with time under isotropic consolidation with different pre-loading steps. For each loading step, as the hydraulic pressure increased, the pore water pressure first increased and then dissipated over time during loading after the hydraulic pressure remained constant. For the specimens under different pre-loading steps, when a total stress of $p = 800$ kPa was applied, the total volumetric strains were almost the same, indicating that the pre-loading had little effect on the total deformation of the reconstituted soil under isotropic consolidation. This may be due to the fact that the sample is in a three-dimensional spherical stress state during the isotropic consolidation process. No matter how the confining the pressure pre-loading steps are, as long as the final confining pressure is the same, the direction and degree of structural adjustment of the soil are roughly the same, so the final volume strain generated by the sample is the same.

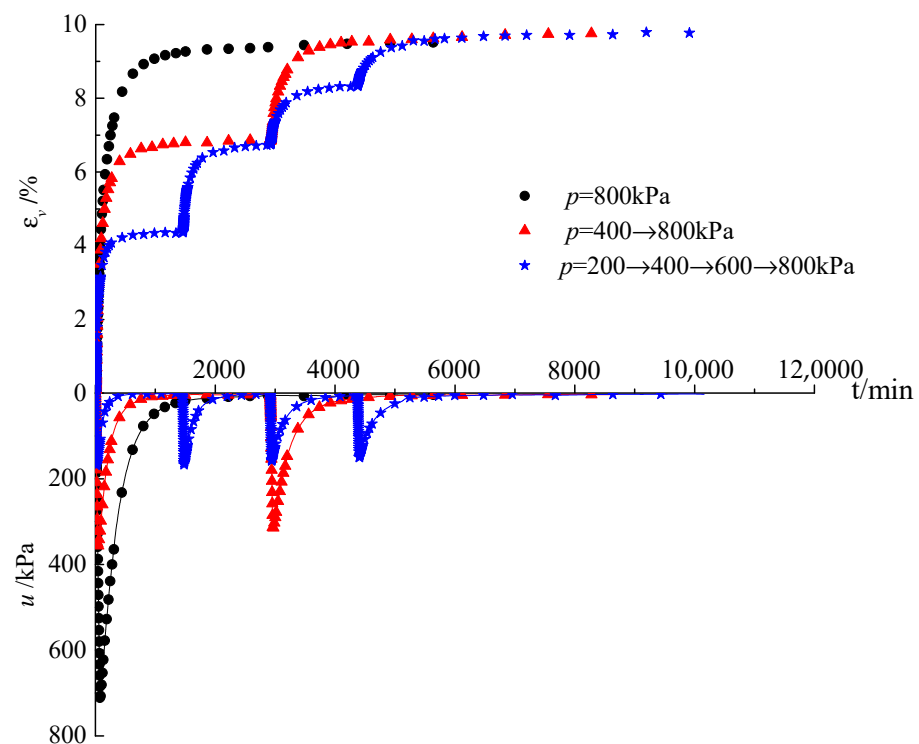


Figure 4. Variation in volumetric strain/pore water pressure over time.

Figure 5 presents the results of the undrained triaxial shear tests on the specimens after creep under different pre-loading steps. In the case of approximately the same

previous total volumetric strain, the specimens were consistently sheared to failure at about $q_f = (\Delta\sigma_1 - \Delta\sigma_3)_f = 750$ kPa. The figure also shows that the pre-loading steps had little effect on the undrained shear strength of the specimen after creep.

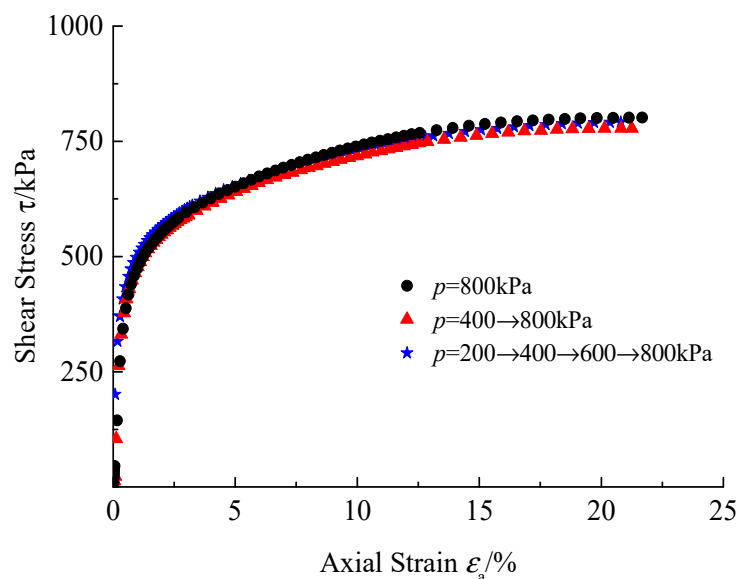


Figure 5. Undrained triaxial shear test after creep under isotropic consolidation.

4.2. Effect of Preloading Steps on Silty Clay under Triaxial Compression

Figure 6 shows the development of deviatoric strain ($\varepsilon_a - \varepsilon_r$) and the variation in pore water pressure over time under triaxial compression with three different pre-loading steps. For each loading step, as the vertical pressure increased, the pore water pressure first increased and then dissipated during loading after the total stress remained unchanged. For the specimens under different pre-loading steps, the application of a final stress of $q = \sigma_1 - \sigma_3 = 360$ kPa produced different total deviatoric strains, and more pre-loading steps yielded lower deviatoric strains, indicating that the pre-loading helps to reduce the time-dependent shear deformation of reconstituted silty clay. This is in agreement with the observations from the multi-stage consolidation tests on reconstituted silty clay conducted by Wu et. al. [13].

To further investigate the influence of different pre-loading steps and the creep effect on the shear strength of the specimens, all specimens were directly subjected to undrained triaxial shear tests to failure after completing the final stage of the triaxial compression creep test. Figure 7 gives the variation in the shear stress τ vs. the axial strain ε_a . It is obvious that the preloaded specimens exhibited higher undrained strengths than those under less pre-loading steps. The undrained triaxial shear strength of the specimen after four-stage deviatoric stress creep was relatively high, followed by two-stage deviatoric stress creep, and finally, one-time applied deviatoric stress creep. The reason is that due to the existence of deviatoric stress in the shear creep process, the soil particles will be continuously adjusted to withstand the action of deviatoric stress. Different pre-loading steps will change the direction of particle adjustment, thus showing that the strength of the soil has changed macroscopically. This is in accordance with the findings by Teresa M. Bodas Freitas et al. [32], who studied the effect of the creep on the short-term bearing capacity of pre-loaded foundations, and pointed out that the time-dependence of soil was responsible for the significant increase in bearing capacity.

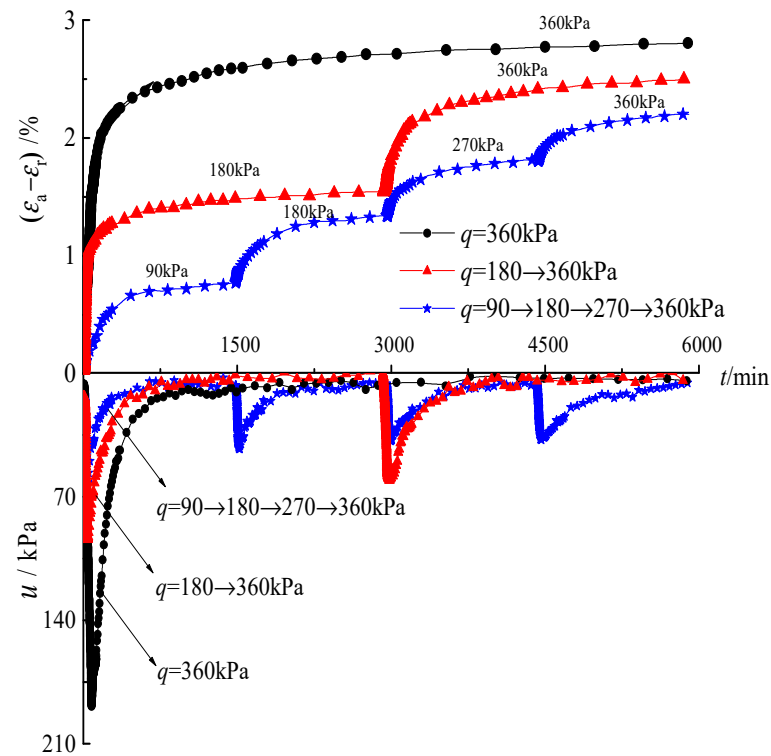


Figure 6. Variation in deviatoric strain/pore water pressure over time.

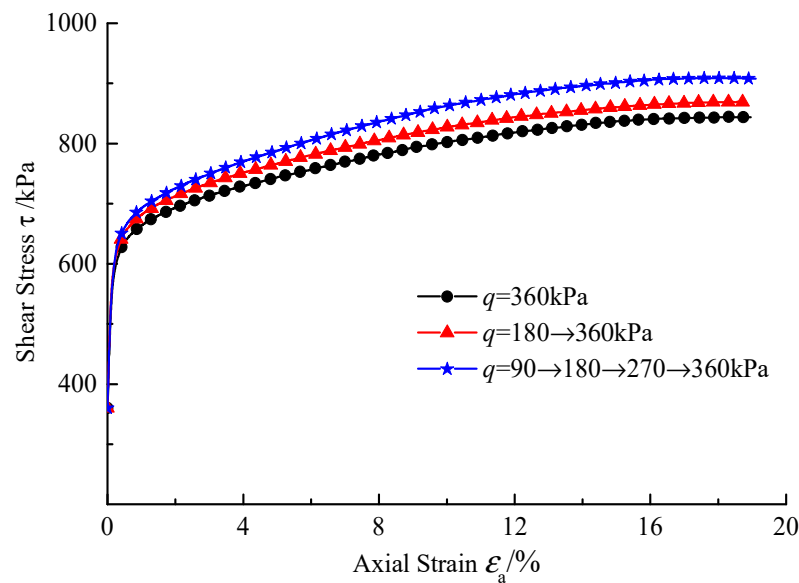


Figure 7. The deviatoric stress–axial strain curve of the samples in the undrained triaxial shear test following triaxial shear creep.

5. Soil Creep under Effective Stress

Based on the principle of effective stress, soil deforms and fails due to effective stresses applied to the skeleton of soil. For this consideration, creep (defined as secondary compression) of the soil may start when the excess pore water pressure dissipates. To determine the time at which specimen consolidation ends (t_{100}), a reference can be used to the change curves of the pore water pressure displayed in Figures 4 and 6. Before t_{100} , the specimens deformed with increasing effective stress; after t_{100} , the specimens creep when the applied total stress was transformed into effective stress. In this study, t_{100} was

determined when the pore water pressure dissipated by more than 95% ($(u_0 - u)/u_0 = 95\%$). Table 2 gives the t_{100} values in the tests under the different loading steps. It can be seen that, for the isotropic consolidation creep test, the t_{100} values at $p = 800$ kPa were close to each other for different pre-loading histories; for the triaxial compression creep test, the t_{100} values at $q = 360$ kPa varied considerably. This indicates that the higher the applied shear stress, the longer the time required for the pore water pressure to dissipate. This suggests that the pre-loading has a greater effect on the sheared specimens than on the isotropic consolidated ones.

Table 2. t_{100} values determined by pore pressure dissipation ($(u_0 - u)/u_0 = 95\%$).

Loading	v_0	Steps	Mean Stress p /kPa	t_{100} /min	v_c	Loading	v_0	Steps	Deviatoric Stress q /kPa	t_{100} /min	v_c
Isotropic consolidation	1.668	One	800	1100	1.5075	Triaxial compression	1.668	One	360	690	1.6482
	1.668	Two	400	700	1.5067		1.668	Two	180	800	1.6470
			800	1150					360	1300	
	1.668	Four	200	350	1.5053		1.668	Four	90	400	1.6450
			400	650					180	600	
			600	700					270	750	
			800	800				360	1290		

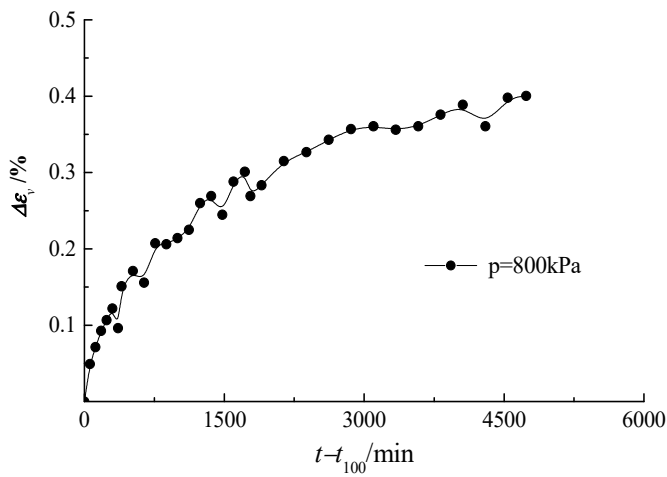
Note: The specific volume v is defined as $v = 1 + e$, v_0 denotes the initial specific volume of the specimen, and v_c indicates the specific volume of the specimen after creep completion.

By analyzing the changes in the specific volume (v) of the specimens in Table 2, it was found that for both the isotropic consolidation creep tests and the triaxial compression creep tests, the specific volume of each specimen decreased under the same stress level, but the differences were relatively close. Under the action of a certain stress, the pores were compressed, causing the internal structure of the specimens to become more compact, which can enhance the strength and stability of the specimens. This also indicates that the effect of the pre-loading steps on the specific volume of the soil samples was not significant.

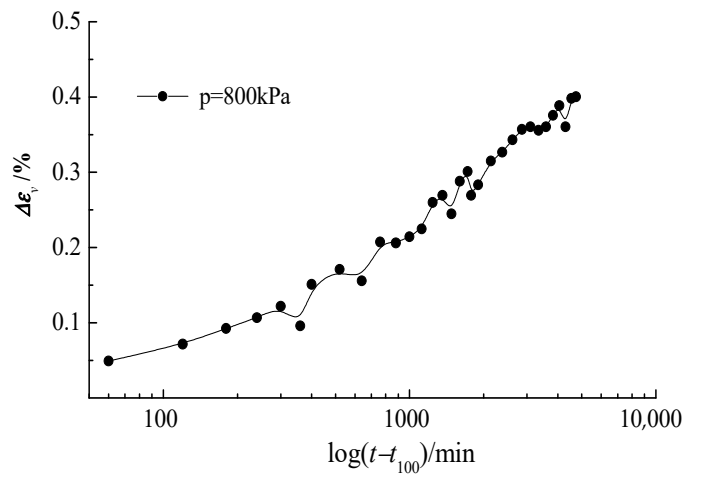
The creep curves of the reconstituted silty clay in isotropic consolidation and triaxial compression under effective stress are shown in Figures 8 and 9, respectively. It can be found from Figures 8(1) and 9(1) that the creep strain evolved non-linearly over time under different stress levels, and that the creep strain under the same Δq increment obviously decreased if there was a preload. However, the preload in isotropic consolidation did not seem to have a significant effect on the secondary volumetric creep strain. Figures 8(2) and 9(2) present the variation in creep strain vs. logarithmic time. It can be observed that the relationship was still non-linear, but the later parts of the curves can be assumed to be linear.

As indicated in Figures 8(1c,2c) and 9(1c,2c), the creep strains under four-stage loading continuously increased within the period with constant stress. This suggests that, for soil creep under an effective stress state and under several loading steps, the time interval for each loading step should be extended to cover the period in which the creep strain rate tends to level off.

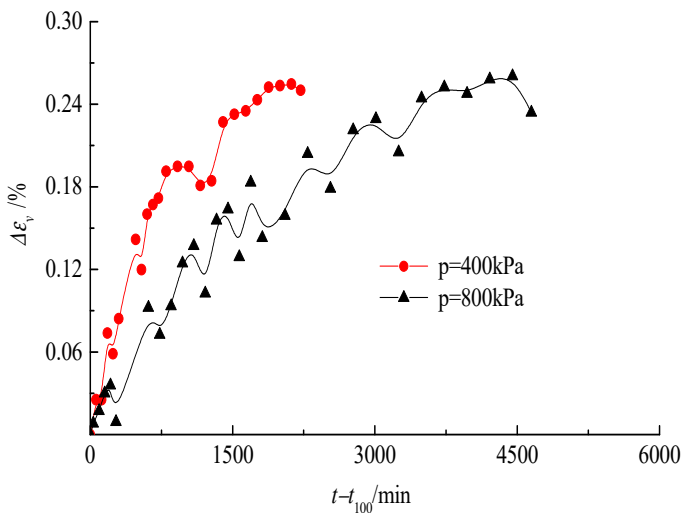
The fluctuation of the creep curves indicates the influence of temperature and implies the importance of temperature control for testing soil creep. Maria Esther Soares Marques et al. [21] detailed the effect of temperature on the viscous behavior of soils.



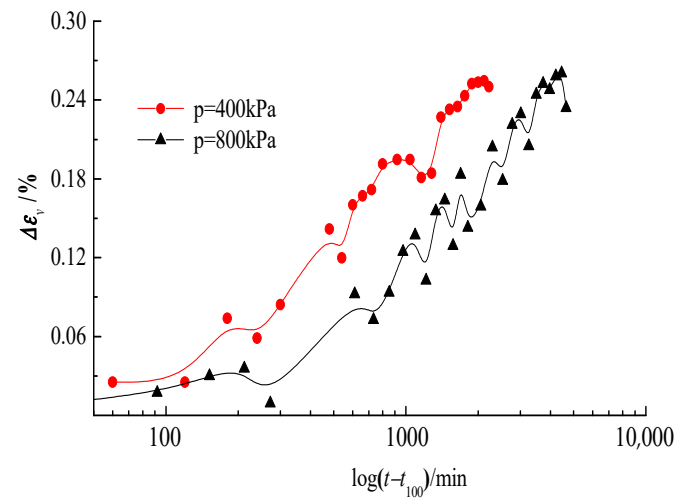
(a) 1-stage loading



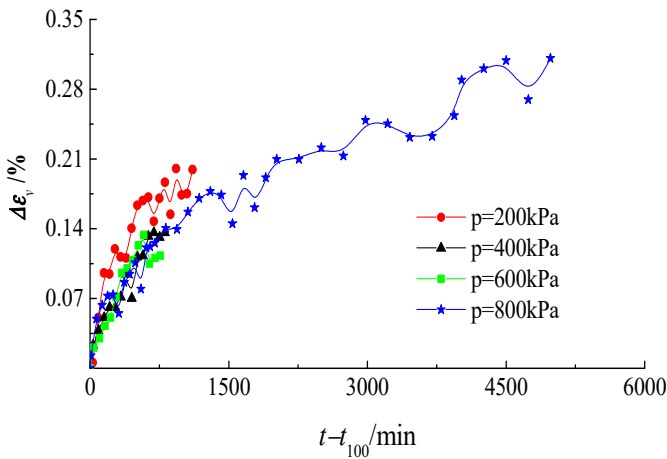
(a) 1-stage loading



(b) 2-stage loading

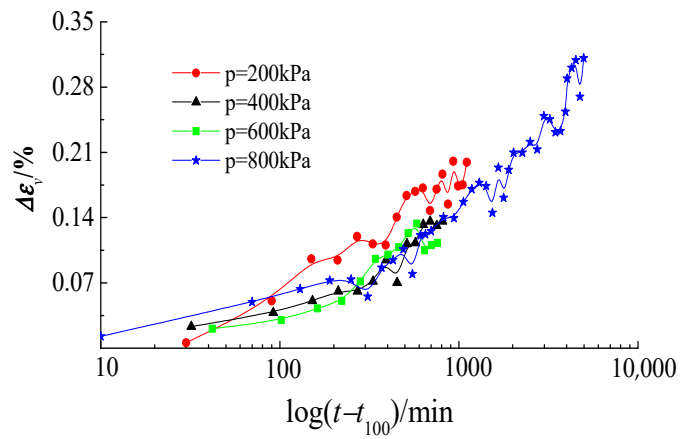


(b) 2-stage loading



(c) 4-stage loading

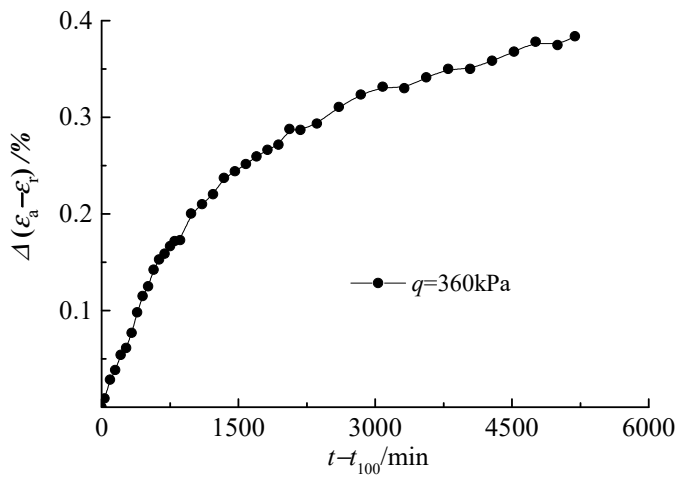
(1) $\Delta\varepsilon_v - (t - t_{100})$



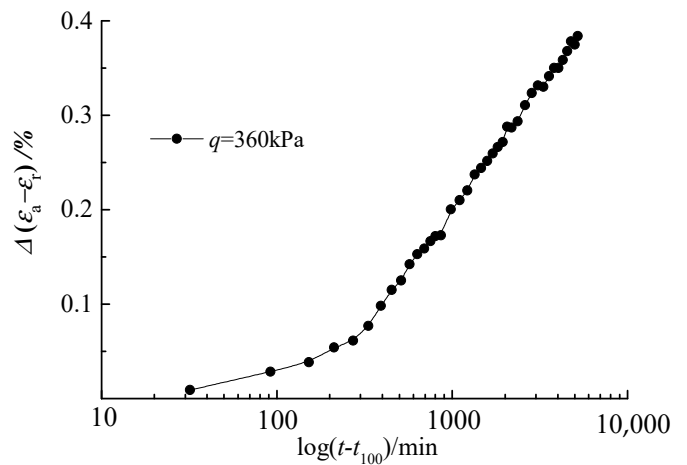
(c) 4-stage loading

(2) $\Delta\varepsilon_v - \log(t - t_{100})$

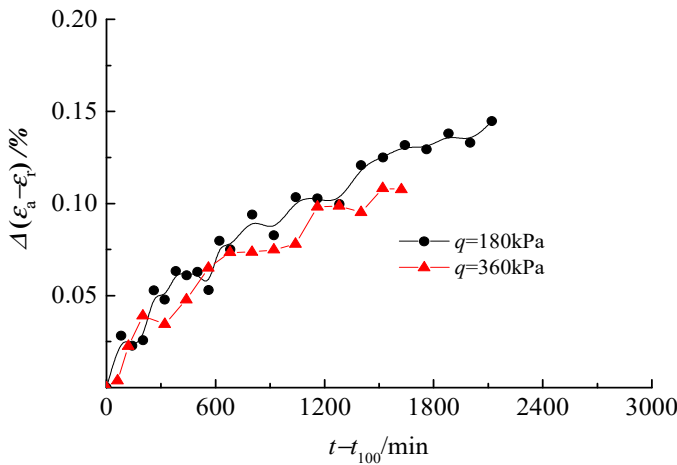
Figure 8. Silty clay creep under isotropic consolidation.



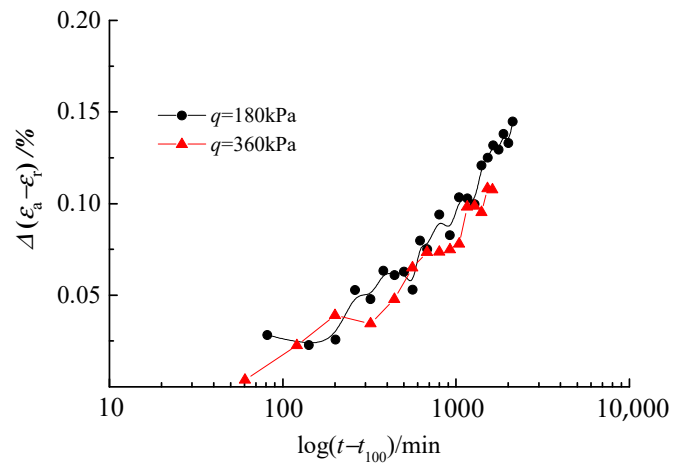
(a) 1-stage loading



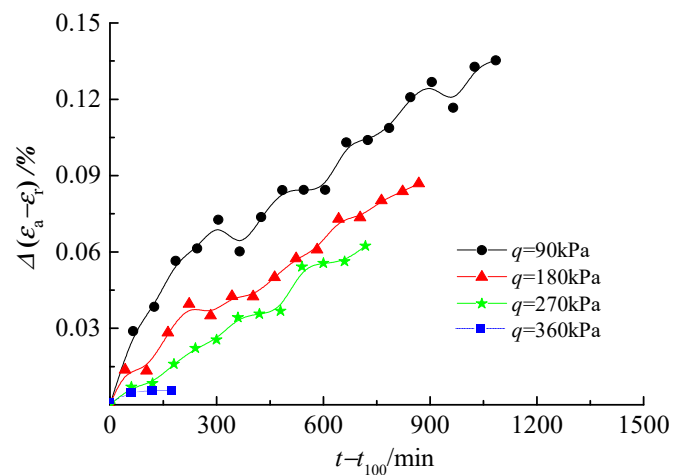
(a) 1-stage loading



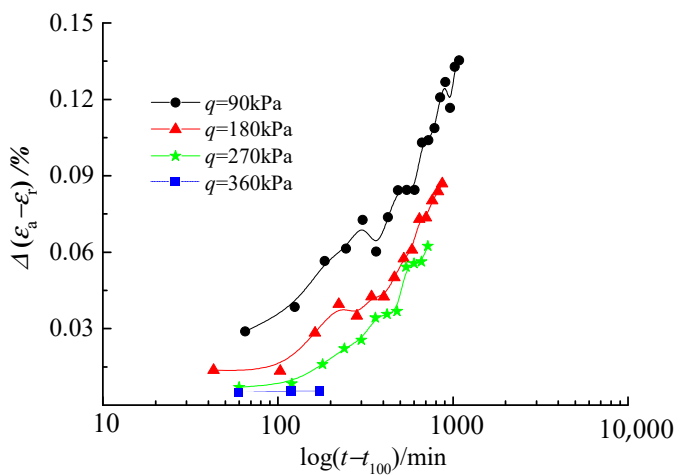
(b) 2-stage loading



(b) 2-stage loading



(c) 4-stage loading



(c) 4-stage loading

(1) $\Delta(\epsilon_a - \epsilon_r) - (t - t_{100})$

(2) $\Delta(\epsilon_a - \epsilon_r) - \log(t - t_{100})$

Figure 9. Silty clay creep under triaxial compression.

6. Creep Model of Reconstituted Silty Clay

6.1. Non-Linear Logarithmic Creep Model

In engineering practice, the time-dependent behavior of soils is commonly characterized by the coefficient of secondary compression, C_α , which can be calculated from consolidation tests by assuming a linear relationship between the void ratio (or settlement) and the logarithm of time. However, this assumes that the creep develops infinitely with time. Based on consolidation tests on reconstituted marine clay, Yin [29] proposed a non-linear logarithmic creep model, which can overcome the above problems, and it is expressed as

$$\Delta\varepsilon_a = \frac{\psi'_0 \ln[(\Delta t + t_0)/t_0]}{1 + (\psi'_0/\Delta\varepsilon_1) \ln[(\Delta t + t_0)/t_0]} \quad (1)$$

where $\Delta\varepsilon_a (= \varepsilon_a - \varepsilon_{a100})$ and Δt are the vertical strain increment and the time increment, respectively; ε_a and t are the total vertical strain and the total time, respectively; ε_{a100} and $t_0 = t_{100}$ are the vertical strain at the end of consolidation and the time, respectively; ψ'_0 and $\Delta\varepsilon_1$ are two creep parameters which can be determined according to the tests. ψ'_0 is related to the initial strain rate C_α .

To use Yin's non-linear creep model, Equation (1) can be rewritten as

$$\Delta\varepsilon_v = \frac{\psi'_0 \ln[(\Delta t + t_0)/t_0]}{1 + (\psi'_0/\Delta\varepsilon_1) \ln[(\Delta t + t_0)/t_0]} \quad (2)$$

It can be further transformed as

$$\frac{\ln[(\Delta t + t_0)/t_0]}{\Delta\varepsilon_v} = \frac{1}{\psi'_0} + \frac{1}{\Delta\varepsilon_1} \ln \frac{\Delta t + t_0}{t_0} \quad (3)$$

where ε_v is the volumetric strain in the isotropic consolidation creep test.

$$\Delta\varepsilon_v = \varepsilon_v - \varepsilon_{v100} \quad (4)$$

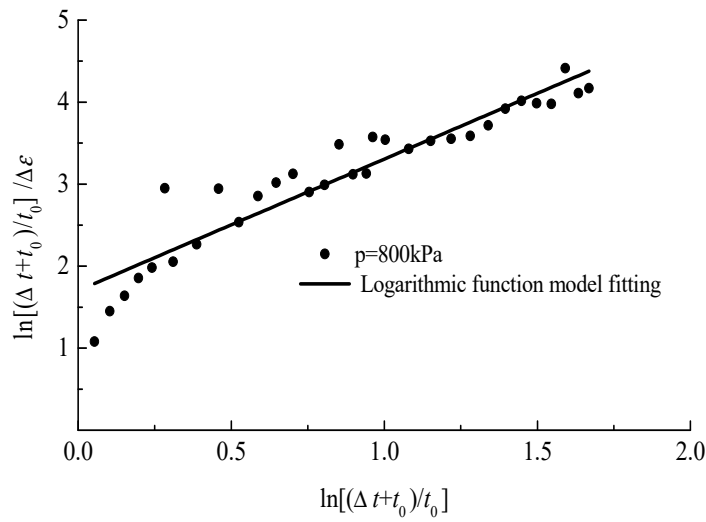
$$\Delta t = t - t_{100} \quad (5)$$

Figure 10(1) shows the best-fitted lines in double-logarithmic coordination for the creeps under isotropic consolidation. Table 3 gives the parameters of the model. Even though the non-linear creep model did not fit very well for the isotropic consolidation creep test, the fitted parameters ψ'_0 (0.2205–0.5875) and $\Delta\varepsilon_1$ (0.4804–0.8390) varied within narrow ranges for $p = 800$ kPa.

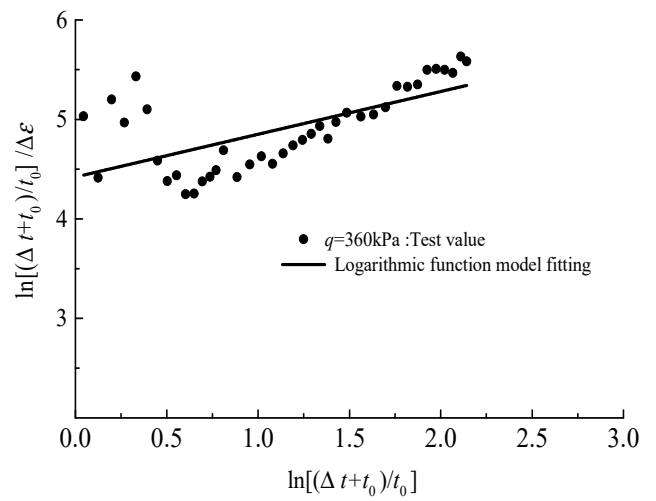
By substituting $(\varepsilon_a - \varepsilon_r)$ for ε_a in Equation (1), the non-linear creep model can be applied to the triaxial compression tests, as shown in Figure 10(2). The fitting parameters are given in Table 3. Also, the non-linear creep model seemed to be less consistent with the deviatoric strain development in the triaxial compression test, especially in the tests with preloading. The parameters $\Delta\varepsilon_1$ (0.0053–2.3256) varied within a wide range for $q = 360$ kPa.

Table 3. Fitting parameters for the non-linear creep model.

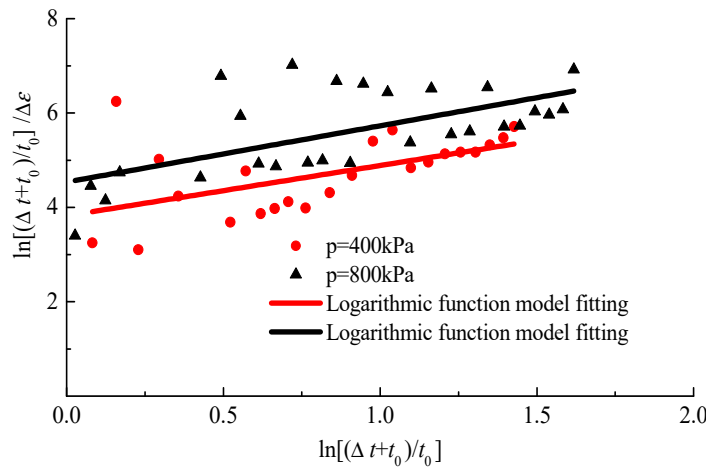
Loading	Mean Stress/kPa	ψ'_0	$\Delta\varepsilon_1$	R^2	Loading	Deviatoric Stress/kPa	ψ'_0	$\Delta\varepsilon_1$	R^2
Isotropic consolidation	800	0.5875	0.6239	0.890	Triaxial compression	360	0.2262	2.3256	0.419
	400	0.2640	0.9179	0.308		180	0.1650	0.3771	0.446
	800	0.2205	0.8390	0.3842		360	0.1594	1.0411	0.016
	200	0.2857	0.3471	0.754		90	0.1582	0.3009	0.584
	400	0.2994	0.2692	0.501		180	0.1176	0.3316	0.197
	600	0.2847	0.3097	0.496		270	0.0685	−0.1749	0.296
	800	0.2954	0.4804	0.638		360	0.5241	0.0053	0.998



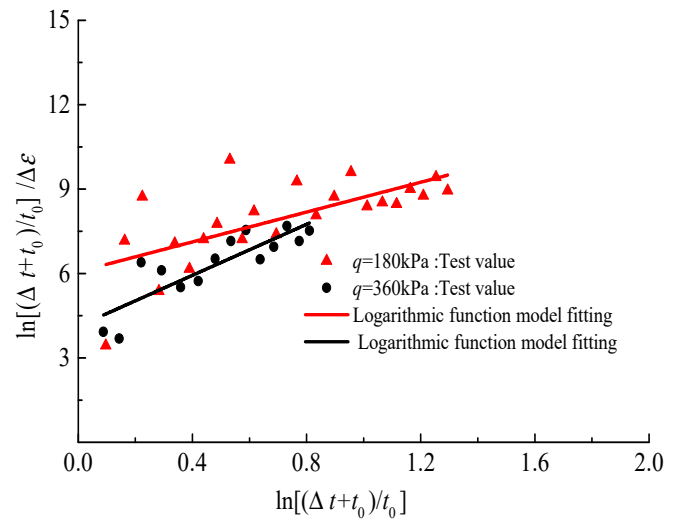
(a) 1-stage loading



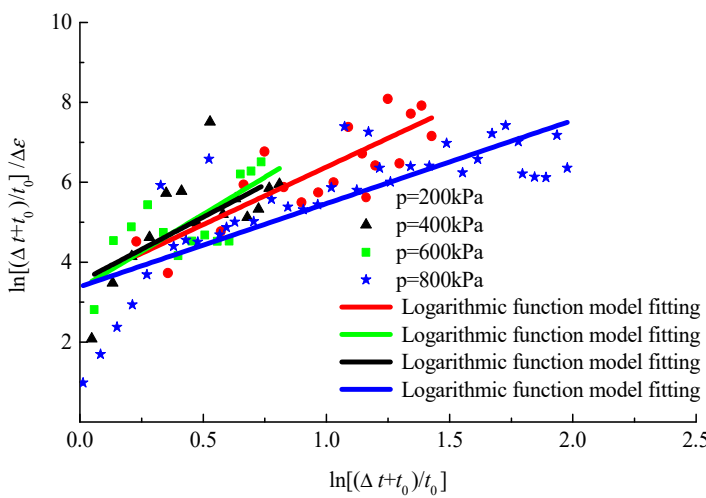
(a) 1-stage loading



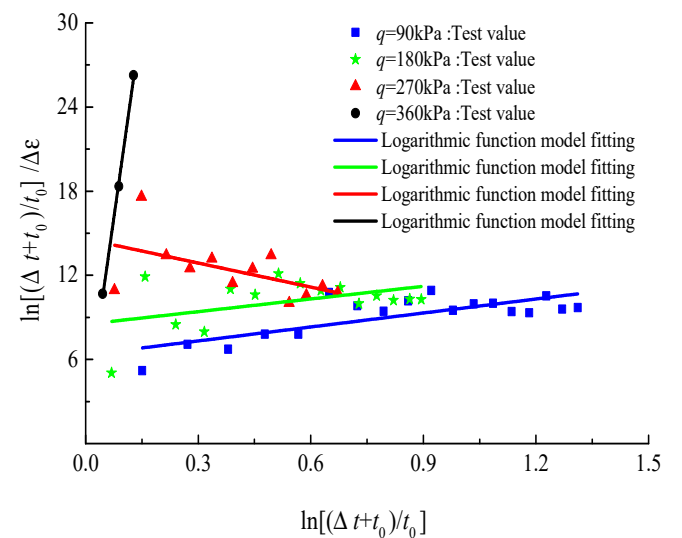
(b) 2-stage loading



(b) 2-stage loading



(c) 4-stage loading
(1) Isotropic consolidation



(c) 4-stage loading
(2) Triaxial compression

Figure 10. Non-linear logarithmic creep model fitting results.

6.2. Hyperbolic Model

According to Figure 8(1) and Figure 9(1), a non-linear hyperbolic model for isotropic consolidation can be proposed:

$$\Delta\varepsilon_v = \frac{\Delta t}{a + b\Delta t} \tag{6}$$

It can be transformed to

$$\frac{\Delta t}{\Delta\varepsilon_v} = a + b\Delta t \tag{7}$$

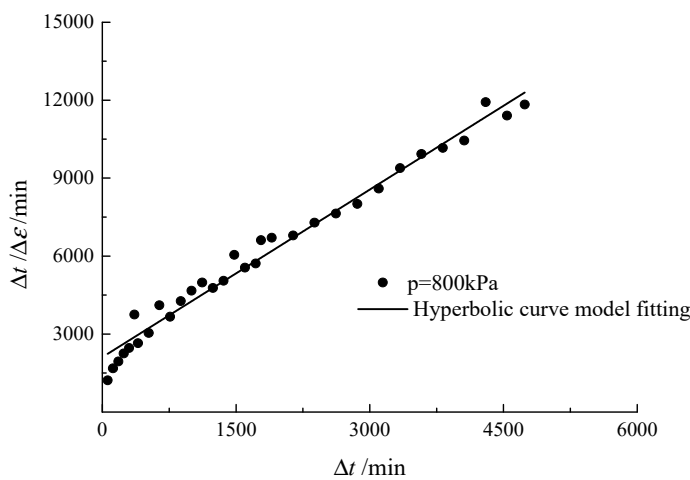
where a and b are two parameters to be determined according to the test creep data. Here, a is assumed to be the inverse of the initial strain rate of creep and b can be the inverse of an attenuation factor of the strain rate over time.

Figure 11(1) shows the lines fitted by the hyperbolic model to the creep curves under isotropic consolidation. It can be observed that the hyperbolic model could better fit the creep curves under different loading steps than the non-linear logarithmic model (Equation (3)). Table 4 gives the fitting parameters of the hyperbolic model. It indicates that the parameters a and b depend on the loading steps and need further studies.

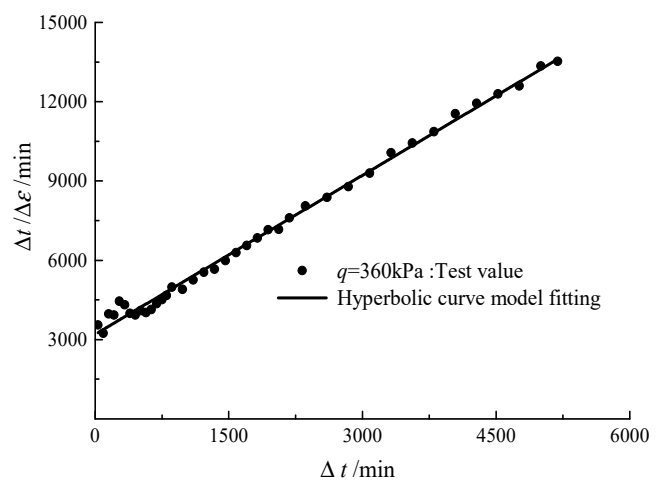
By substituting $(\varepsilon_a - \varepsilon_r)$ for ε_v in Equation (7), this model can also be used for the triaxial compression test. Figure 11(2) shows the fitted lines of the creep curves under triaxial compression. The results indicate that this hyperbolic model can better fit the triaxial compression curves. The fitting parameters of a and b are given in Table 4. Parameter b , which is assumed to be inversely proportional to the attenuation factor of strain rate, varied from 2.005 to 190.04 for creep at $q = 360$ kPa, which indicates that the preload in triaxial compression may have a significant effect on the creep behavior of silty clay under shearing.

Table 4. Fitting parameters for the hyperbolic creep model.

Loading	Mean Stress/kPa	a	b	R^2	Loading	Deviatoric Stress/kPa	a	b	R^2
Isotropic consolidation	800	2108.4	2.150	0.980	Triaxial compression	360	3199.1	2.005	0.995
	400	2673	2.638	0.906		180	5234.1	4.790	0.901
	800	6885.4	2.381	0.724		360	7938.6	4.062	0.925
	200	1304.3	4.180	0.930		90	2907.2	5.282	0.882
	400	2375	4.723	0.720		180	5467.7	5.984	0.665
	600	2432.2	4.895	0.773		270	11131	0.487	0.580
	800	3449.1	2.936	0.925		360	2441.8	190.04	0.998



(a) 1-stage loading



(a) 1-stage loading

Figure 11. Cont.

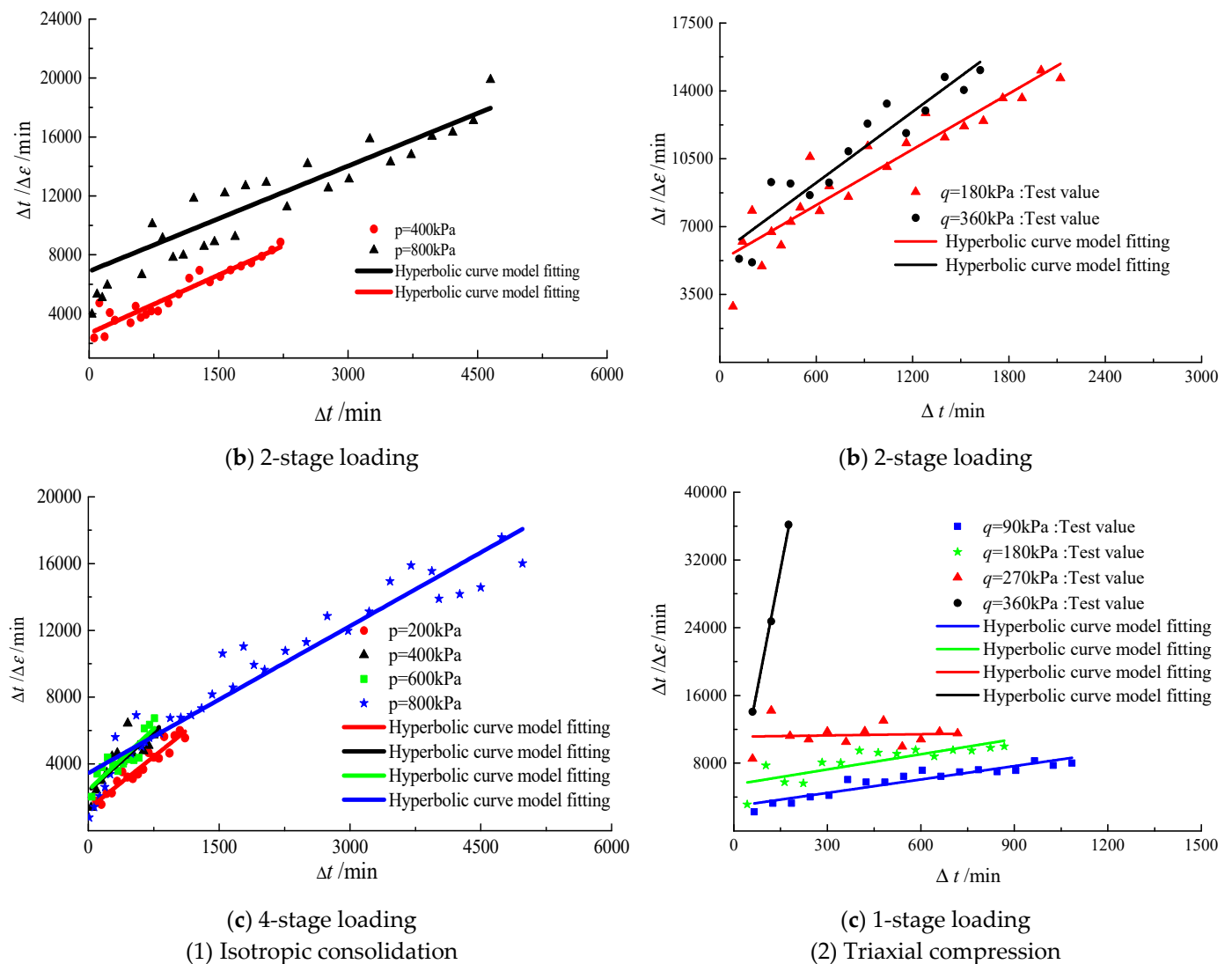


Figure 11. Hyperbolic creep model fitting results.

7. Discussions

7.1. Creep of Silty Clay

The time-dependence of soil involves the occurrence of creep under a constant stress state. In engineering practice, the stress state of a soil element can be considered as constant after construction/excavation. It seems sound to study soil's creep behavior under a constant total stress state based on the condition that the soil material is assumed to be continuous, and when the overall deformation of the soil is of interest.

In this study, Figures 4 and 6 present the overall strain development over time. It is clear that the pre-loading steps had different effects on strain development under different loading paths. For isotropic consolidation, the overall volumetric strain of the reconstituted silty clay specimen responded only to the total mean stresses but not to the pre-loading steps, while for triaxial compression, the overall deviatoric strain was sensitive to the pre-loading steps.

However, due to the excess pore water pressure induced by the applied stresses in the silty clay specimens, the effective stresses may change with the dissipation of the pore water pressure. Therefore, the overall deformation after the total stress is applied involves both consolidation compression and secondary compression (creep). The primary consolidation can be solved by the theory of soil consolidation, while the creep description in this study focuses on secondary compression.

7.2. The Determination of t_{100}

For creep description, the division of the consolidation and the secondary compression are vital. It is assumed that the primary consolidation is controlled by the dissipation of the excess pore water pressure induced by loading, while the secondary compression is attributed to the skeleton adjustment of the soil after the total stress is entirely transformed into effective stresses. However, in the real world, it is impossible to separate these two processes at the same time. At a high degree of consolidation, i.e., $u/u_0 < 10\%$, the dissipation of pore pressure slows down and the skeleton adjustment controls the deformation rate, which in turn may affect the pore pressure dissipation. Taking this into consideration, the division time of the primary consolidation and the secondary compression can be selected before the pore pressure entirely dissipates.

In this study, a consolidation degree of 95% was used to determine t_{100} , whose validity needs to be demonstrated by various creep models.

7.3. The Creep Models for Silty Clay

The characteristics of the soil's creep strain over time give the hint of a non-linear model. Two models with simple parameters, i.e., the non-linear logarithmic model proposed by Yin [29] and the hyperbolic model, were tested in this study. The comparison demonstrated that the hyperbolic model showed a promising ability to describe the creep of the reconstituted silty clay under both isotropic consolidation and triaxial compression. However, the parameters of the model varied over a wide range with the loading steps, and the physical properties of the parameters were not clear. For these reasons, it is recommended that the nature of soil creep be examined by micro-examination methods to provide a sound support for creep models and related parameters.

7.4. The Influence of Pre-Loading Steps on the Creep Behavior of Silty Clay

When a load is applied to the foundation, the induced stress state increment can be divided into two parts, i.e., the mean stress increment Δp and differential stress increment Δq . If it is assumed that the responses of the soil to these two stress states can be superposed, the creep behaviors under these two stress states need to be elucidated separately.

As shown in Figures 4 and 6, the pre-loading steps had an obvious effect on the creep strain development under differential pressures, but had little effect under hydraulic pressure. It can be seen from Table 2 that the pre-loading may prolong the consolidation time under triaxial compression, and that the consolidation time under isotropic consolidation at 800 kPa did not significantly change under different preloads.

Since the undrained strengths of the reconstituted silty clay with creep with pre-shearing (Figure 7) were higher than those without pre-shearing (Figure 5), it can be deduced that the creep under deviatoric stress helps to improve the resistance of silty clay to failure and deformation when the loading path is similar to its pre-loading process. However, the creep under hydraulic pressure may not help to improve the soil's resistance to failure.

The different responses of silty clay to isotropic consolidation and triaxial compression may be related to the structural evolution of the soil. For isotropic consolidation, the force between soil particles is uniformly distributed in different directions, but for triaxial compression, the force distribution may have a dominant direction and induce a degree of anisotropy within the soil structure. This requires more work using discrete element method simulations.

8. Conclusions

Isotropic consolidation and triaxial compression are two typical loading paths for studying silty clay mechanical behaviors. In this study, the effect of preload on soil creep behaviors under these two loading paths was examined through a series of laboratory tests:

- (1) The preload had an obvious influence on the creep behavior of reconstituted silty clay in the triaxial shear creep tests, but had little influence in the isotropic consolidation creep tests.
- (2) The determination of t_{100} is vital to developing a suitable creep model for silty clay. The method of using the dissipation of pore water pressure was effective, but the degree of dissipation related to t_{100} needs further study.
- (3) The hyperbolic model (Equation (6)) proposed in this study can better fit the testing data than the non-linear logarithmic model, but the model parameters are pre-loading-dependent for triaxial compression, and further examination using micro-scale approaches is encouraged.
- (4) This paper focused on the study of the creep response of reconstituted silty clay samples to different pre-loading steps under isotropic consolidation creep tests and triaxial compression creep tests. It was observed that the silty clay samples exhibited different deformation responses under the two distinct loading paths, which may be associated with the structural evolution of the soil samples. This hypothesis awaits further clarification in future research through conducting additional triaxial creep tests on intact soil and the implementation of discrete element numerical simulation (DEM). Further research is crucial for establishing a robust scientific framework to elucidate the intrinsic creep behavior and the underlying mechanisms of silty clay.

Author Contributions: Conceptualization, B.X., P.Z. and S.W.; methodology, B.X.; software, B.X. and P.Z.; validation, B.X., P.Z. and S.W.; formal analysis, P.Z.; investigation, B.X.; resources, P.Z. and S.W.; data curation, B.X. and S.W.; writing—original draft preparation, B.X.; writing—review and editing, P.Z.; visualization, B.X. and P.Z.; supervision, S.W.; project administration, B.X.; funding acquisition, B.X. All authors have read and agreed to the published version of the manuscript.

Funding: This research was financially supported by the National Natural Science Foundation of China (grant No. 51878616), the Fundamental Scientific Research Funds for Universities of Zhejiang Province (grant No. FRF20QN001), and the Visiting Engineer program in Zhejiang Province (grant No. FG2023341).

Data Availability Statement: The data presented in this study are available on request from the corresponding author.

Conflicts of Interest: The authors declare no conflicts of interest.

References

1. Augustesen, A.; Liingaard, M.; Lade, P.V. Evaluation of time-dependent behavior of soils. *Int. J. Geomech.* **2004**, *4*, 137–156. [CrossRef]
2. Zhu, Q.Y.; Yin, Z.Y.; Hicher, P.Y.; Shen, S.L. Nonlinearity of one-dimensional creep characteristics of soft clays. *Acta Geotech.* **2016**, *11*, 887–900. [CrossRef]
3. Bishop, A.W.; Lovenbury, H.T. Creep characteristics of two undisturbed clays. In Proceedings of the 7th International Conference of Soil Mechanics and Foundation Engineering, Mexico City, Mexico; 1969; pp. 29–37. Available online: <https://www.issmge.org/search?keyword=Creep+characteristics+of+two+undisturbed+clays> (accessed on 12 May 2024).
4. Fodil, A.; Aloulou, W.; Hicher, P.Y. Viscoplastic behavior of soft clay. *Geotechnique* **1997**, *47*, 581–591. [CrossRef]
5. Xiao, B. Study on Creep Characteristics and Creep Model of Reconstituted Silty Clay. Master's Thesis, Zhejiang University of Technology, Hangzhou, China, 2017. (In Chinese).
6. Hu, M.; Xiao, B.; Wu, S.; Zhou, P. Research on creep characteristics and creep model of reconstituted silty clay. *Chin. J. Undergr. Space Eng.* **2018**, *14*, 332–340. (In Chinese)
7. Hu, M.; Xiao, B.; Lu, Y.; Zhang, Y.; Zhang, Y. Creep tests and creep model for reconstituted over-consolidated saturated clay. *Chin. J. Geotech. Eng.* **2023**, *45*, 6–10. (In Chinese)
8. Leroueil, S.; Kabbaj, M.; Tavenas, F.; Bouchard, R. Stress strain-strain rate relation for the compressibility of sensitive natural clays. *Geotechnique* **1985**, *35*, 159–180. [CrossRef]
9. Jostad, H.P.; Yannie, J. A procedure for determining long-term creep rates of soft clays by triaxial testing. *Eur. J. Environ. Civ. Eng.* **2022**, *26*, 2600–2615. [CrossRef]
10. Vyalov, S.S.; Khamed, A.S. Creep and long-term strength of clayey soils in triaxial compression. *Soil Mech. Found. Eng.* **1997**, *34*, 9–14. [CrossRef]

11. Wang, Z.; Qiao, L.; Li, S. Research on the influence of load level and void ratio on soil secondary compression properties. *Chin. J. Civ. Eng.* **2013**, *46*, 112–118. (In Chinese)
12. Ze, L.; Ho, Z.; Li, S.; Ch, F. Variation law and quantitative evaluation of secondary consolidation behavior for remolded clays. *Chin. J. Geotech. Eng.* **2012**, *34*, 1496–1500. (In Chinese)
13. Wu, S.; Hu, M.; Zhang, Y.; Xiao, B.; Chen, K. Experimental study on secondary consolidation characteristics of silty clay. *J. Hydraul. Eng.* **2015**, *46* (Suppl. S1), 338–342+348. (In Chinese)
14. Luo, Q.; Chen, X.; Wang, S.; Huang, J. Experimental and empirical model research on deformation aging of soft clay. *Rock Soil Mech.* **2016**, *37*, 66–75. (In Chinese)
15. Chen, X. Consolidation effect of soft soil deposited by sea-land alternating facies. *Chin. J. Geotech. Eng.* **2011**, *33*, 520–528. (In Chinese)
16. Zhou, P. Experimental and Model Study on Triaxial Creep Characteristics of Saturated Cohesive Soil. Master's Thesis, Zhejiang University of Technology, Hangzhou, China, 2018. (In Chinese).
17. Xiao, B.; Hu, M.; Zhou, P.; Lu, Y.; Zhang, Y. Creep behavior of saturated clay in triaxial test and a hyperbolic model. *Geofluids* **2021**, *2021*, 7882046. [[CrossRef](#)]
18. Long, L.; Li, Z.; Li, Y. Investigation of an Empirical Creep Constitutive Model of Changsha Red Loam. *Buildings* **2023**, *13*, 1064. [[CrossRef](#)]
19. Niu, Y.; Cheng, Y.; Wang, X.; Zhang, Y.; Li, Q. Study on dynamic characteristics and non-constant fractional dynamic creep model for frozen silty clay. *Cold Reg. Sci. Technol.* **2024**, *218*, 104086. [[CrossRef](#)]
20. Hu, M.; Xiao, B.; Wu, S.; Zhou, P.; Lu, Y. Creep of Reconstituted Silty Clay with Different Pre-loading. In Proceedings of the China-Europe Conference on Geotechnical Engineering, Vienna, Austria, 13–16 August 2018; Springer Science and Business Media LLC: Berlin/Heidelberg, Germany, 2018; pp. 529–533.
21. Maria, E.; Soares, M.; Serge, L.; de Almeida, M.d.S.S. Viscous behaviour of St-Roch-de-l'Achigan clay. *Can. Geotech. J.* **2004**, *41*, 25–38.
22. Miao, L.; Zhang, J.; Wang, F.; Houston, S.L. Time-dependent deformation behavior of Jiangsu marine clay. *Mar. Georesour. Geotechnol.* **2008**, *26*, 86–100. [[CrossRef](#)]
23. Mesri, G. Coefficient of secondary compression. *Soil. Mech. Div. ASCE* **1973**, *99*, 123–137. [[CrossRef](#)]
24. Newland, P.L.; Allely, B.H. A study of the consolidation characteristics of a clay. *Geotechnique* **1960**, *10*, 62–74. [[CrossRef](#)]
25. Singh, A.; Mitchell, J.K. Creep potential and rupture of soil. In Proceedings of the 7th International Conference of Soil Mechanics and Foundation Engineering, Mexico City, Mexico; 1969; pp. 379–384. Available online: <https://trid.trb.org/view/127110> (accessed on 12 May 2024).
26. Sekiguchi, H. Rheological characteristics of clays. In Proceedings of the 9th International Conference of Soil Mechanics and Foundation Engineering, Tokyo, Japan, 10–15 July 1977; pp. 289–292.
27. Taylor, D.W.; Merchant, W.A. A theory of day consolidation accounting for secondary compressions. *J. Math. Sand Phys.* **1940**, *19*, 167–185. [[CrossRef](#)]
28. Tavenas, M.; Leroueil, F.; La Rochelle, P.; Roy, M. Creep behaviour of an undisturbed lightly overconsolidated clay. *Can. Geotech. J.* **1978**, *15*, 402–423. [[CrossRef](#)]
29. Yin, J.H. Non-linear creep of soil in oedometer tests. *Geotechnique* **1999**, *49*, 699–707. [[CrossRef](#)]
30. Singh, A.; Mitchell, J.K. General stress-strain-time function for soils. *J. Soil Mech. Found. Div.* **1968**, *94*, 21–46. [[CrossRef](#)]
31. Mesri, G.R.; Febres-Cordero, E.; Shields, D.; Castro, A. Shear stress-strain-time behavior of clays. *Geotechnique* **1981**, *31*, 537–552. [[CrossRef](#)]
32. Freitas, T.M.B.; Potts, D.M.; Zdravkovic, L. The effect of creep on the short-term bearing capacity of pre-loaded footings. *Comput. Geotech.* **2012**, *42*, 99–108. [[CrossRef](#)]
33. *ISO 14688-2:2017*; Geotechnical Investigation and Testing—Identification and Classification of Soil—Part 2: Principles for a Classification. International Organization for Standardization: Geneva, Switzerland, 2017.
34. *GB 50007*; Code for Design of Building Foundation. China Architecture & Building Press: Beijing, China, 2011.

Disclaimer/Publisher's Note: The statements, opinions and data contained in all publications are solely those of the individual author(s) and contributor(s) and not of MDPI and/or the editor(s). MDPI and/or the editor(s) disclaim responsibility for any injury to people or property resulting from any ideas, methods, instructions or products referred to in the content.